NUCL SCI TECH (2019) 30:137
https://doi.org/10.1007/s41365-019-0661-8

Evaluation of CdZnTe spectrometer performance in measuring energy spectra during interventional radiology procedure

Lin Chai[1] · Lian Chen[2] · Cui-Ping Yang[1] · Dong-Dong Zhou[1] · Meng-Meng Yang[1] · Wei-Wei Qu[1,3] · Gao-Long Zhang[4,5] · Da-Qian Hei[6] · Shou-Ping Xu[7] · Xin-Jian Chen[1]

Received: 13 February 2019 / Revised: 11 June 2019 / Accepted: 22 June 2019 / Published online: 12 August 2019

Abstract Interventional radiology has been beneficial for patients for over 30 years of age with the combination of diagnostic and therapeutic methods. The radiation affecting occupationally exposed workers should be evaluated by means of the energy spectra and flux of X-rays in the treatment room. The present study aims to obtain the energy spectra of interventional procedures and study the capability of some detectors to evaluate the dose in interventional procedures. These measurements were taken by silicon-drift, CdTe, and CdZnTe detectors. The energy spectra were corrected by the energy-response curve of each detector. The energy-response curves of silicon-drift and CdTe detectors provided by the manufacturers specification were used. The energy response of the CdZnTe detector was measured by ^{133}Ba and ^{152}Eu γ sources. The experimental data were compared with the simulation results, and their perfect agreement provides a way to correct the energy or dose response, which can be used for the personal dosimeter developed by our group. Moreover, the measured energy spectra can be used in individual radiation protection. The present study shows that the CdZnTe detector is a good candidate detector in interventional procedures.

Keywords Interventional radiology procedures · Energy-response curve · Energy spectrum · Radiation protection

1 Introduction

Interventional procedures using ionizing radiation have revolutionized medicine in the last few decades for diagnosis, therapy, and palliation, resulting in the ability to offer to many patient treatments that were not possible

L. Chai and L. Chen have contributed equally to this work.

This work was supported by the National Natural Science Foundation of China (No. 11705123), Natural Science Foundation of Jiangsu Province (No. BK20160306), China Postdoctoral Science Foundation (No. 2016M591911), and the Project of the State Key Laboratory of Radiation Medicine and Protection, Soochow University (No. GZN1201801).

✉ Wei-Wei Qu
wwqu@suda.edu.cn

Gao-Long Zhang
zgl@buaa.edu.cn

1 State Key Laboratory of Radiation Medicine and Protection, School of Radiation Medicine and Protection, Soochow University, Suzhou 215123, China

2 State Key Laboratory of Particle Detection and Electronics, University of Science and Technology of China, Hefei 230026, China

3 Collaborative Innovation Center of Radiological Medicine of Jiangsu Higher Education Institutions, Suzhou 215123, China

4 School of Physics and Nuclear Energy Engineering, Beihang University, Beijing 100191, China

5 Beijing Advanced Innovation Center for Big Data-Based Precision Medicine, Beihang University, Beijing 100083, China

6 College of Materials Science and Engineering, Nanjing University of Aeronautics and Astronautics, Nanjing 211106, China

7 Department of Radiation Oncology, PLA General Hospital, Beijing 100853, China

previously [1]. However, it is associated with high radiation doses to patients and staff, due to extended fluoroscopy times and the large number of radiographs. The need for measurement and evaluation of patient and staff doses is apparent [2].

The skin dose received by the patients was studied by Barrera-Rico et al. [3]. They used the Gafchromic XR-RV3 film and TLDs to determine the entrance surface dose in patients who undergo interventional radiology procedures. These doses were evaluated from the direct exposure; however, the scattered radiation occupies all of the treatment rooms and contributes to eye, thyroid, skin, and other organ doses. To evaluate the doses received by the staff and explore effective protection, the energy spectrum of scattered X-rays should be measured.

For X-ray detection, several detectors have been used, such as the Si (Li) detector, silicon-drift detector (SDD), and CdTe and CdZnTe detectors. The Si(Li) detector exhibits good energy resolution; however, its low efficiency and need of cooling make it unsuitable for many cases [4]. CdTe and CdZnTe detectors [5–7] show worse energy resolutions than the Si(Li) detector. However, the detection efficiencies of CdTe and CdZnTe detectors are much higher than that of Si (Li) detector. Moreover, the possible usage in room temperature makes it more suitable in many applications than Si (Li) detector. Therefore, SDDs [8, 9] which combine a large sensitive area with a small value of the output capacitance are well suited for high resolution and X-ray spectroscopy with high counting rate. Servoli et al. [10, 11] studied the CMOS active pixel sensors as potential detectors for diffused X-rays during interventional radiology procedures, which cover an energy range from 15–20 keV to several tens keV. The detector response showed less than 5% precision with respect to the other commercial active dosimeters. In recent years, CdZnTe detectors have been widely used in the measurement of X- and γ-rays in national security, medical imaging, and astrophysics because of their excellent characteristics: high mean atomic number ($Z \approx 50$), high density ($\rho = 5.78$ g/cm^3), and high band gap ($E\text{g} = 1.57$ eV), combined with high resistivity [12]. Here, the possibility of a CdZnTe detector for applications in interventional procedures needs to be studied. To evaluate performance of CdZnTe detector in interventional procedures, the measurement was compared with that of several commercial X-ray spectrometers, such as SDD and CdTe. CdZnTe detector is very suitable to the personal dosimeter which can cover the energy range of 10–1500 keV, the energy-response curves are crucial. A personal dosimeter based on the CdZnTe detector is being developed by our group. Tomal et al. [13] studied the energy-response functions of Si(Li), SDD, and CdTe detectors in the mammographic energy range (5–40 keV) through Monte Carlo simulation. The simulation for the energy-response curve of CdZnTe detector was performed in Ref. [14] during the measurement of high dose rate response to X-ray. There are no experimental studies about the energy-response curve for CdZnTe detector. This is very important for the concerned applications. On the basis of this consideration, this paper studied the energy response of the CdZnTe detector experimentally; thus, it provides the reference data for the application of CdZnTe detectors.

This paper is organized as follows. Section 2 describes the experimental procedure. The data analysis and discussions are presented in Sect. 3. The summary is given in Sect. 4.

2 Experiment

To measure the environmental energy spectrum of interventional radiology procedure, a CdZnTe detector and two commercial spectrometers were used. The SDD (Amptek, X-123SDD) covers the energy range from several keV to 30 keV [15], and the CdTe detector (Amptek, X-123CdTe) detects the X-rays with energy higher than 30 keV [16]. Because the single detector used above cannot cover the whole energy range, two detectors were used in the measurement. The X-123SDD and X-123CdTe spectrometers can be controlled by the Amptek ADMCA display and acquisition software. This software completely controls and configures the detectors and downloads and displays the data. The CdZnTe detector (Imdetek, DT-01C1) has a wider energy range from 10 keV to 1.5 MeV [17]. The output of CdZnTe detector was readout by preamplifier module. The amplified signal by spectroscopy amplifier was connected to a waveform digitizer (CAEN DT5730 Desktop Digitizer, eight channels, 14 bits, 500 MHz) to record the waveform of each event. The waveform was analyzed along the given gated time; therefore, the pulse height of the γ rays in the CdZnTe detector can be obtained via DPP-PHA firmware. The geometry size of the CdZnTe detector is $10 \times 10 \times 5$ mm^3. The operation voltage of CdZnTe detector is $-$ 2000 V. Before the measurement, CdTe and CdZnTe detectors were calibrated by using γ sources including ^{241}Am, ^{133}Ba, ^{137}Cs, ^{22}Na , and ^{60}Co sources. The SDD was calibrated by an X-ray tube by adjusting the high voltage and changing the filters to produce the characteristic energies of some elements (Al: 1.49 keV, Ti: 4.51 keV, Cu: 8.04 keV, Mo: 17.44 keV). The experiment was performed on a Siemens Artis Zee multi-purpose system where the X-ray tube and image intensifier are mounted on a C-arm. Here, a phantom was used during the experiment. The voltage and current of this high-voltage generator were adjusted automatically depending on the phantoms used to obtain a better image quality. The high voltage for the tube is set to 73.0 kV and the current is 105.6 mA, which are very similar to those in practical situations. The dose rate is approximately 56.6 mGy/h. To study the dependence of distance for scattered X-ray radiation, the detectors were placed at several points with the distance to the edge of radiation field. The distance range covered from 0 to 200 cm.

The energy-response curve of the CdZnTe detector is primary for the personal dosimeter development. This energy-response curve can be explained by the relative efficiency of given detector. In practical use, several CdZnTe detectors with different geometry sizes were used in the dosimeter development. To obtain the energy response more conveniently, the simulation was used. The simulation was performed by the Geant4 toolkit [18]. On this basis, the relative efficiencies should be compared with the experimental measurement to evaluate the simulation. Furthermore, the energy spectra during in interventional radiology procedures should be corrected.

Here, in the simulation the component of CdZnTe detector is $Cd_{0.9}Zn_{0.1}Te$, the average atomic number is 49.1, and the density is 5.78 g/cm^3. In the simulation, the aluminum entrance window with a thickness of 0.5 mm for the CdZnTe detector was taken into account. The γ rays were emitted from a plane source and hit the detector perpendicularly. The energy range was from 10 keV to 1.5 MeV. The photoelectric, single Compton scattering, and electron pair effects were taken into account in the electromagnetic procedure physics list. The number of each physical interaction type was recorded. Because the main mechanism of low-energy X-rays in the CdZnTe detector is the photoelectric effect, the number of particles with the photoelectric effect was compared with the full-energy peak area. Here, the geometry size of the CdZnTe detector in the simulation is $10 \times 10 \times 5$ mm^3.

3 Results and discussion

The data were analyzed within the ROOT data analysis framework [19]. First, the energy resolution was also obtained with γ sources, including ^{137}Cs, ^{22}Na, and ^{60}Co, in our measurements. The peak area for each energy peak was fitted by the Gaussian function. The energy resolutions were obtained and are listed in Table 1. This shows that the energy resolution can reach 1.34% at 1112 keV for ^{152}Eu. For low energy, such as 39.4 keV of ^{152}Eu and 59.5 keV of ^{241}Am, it is approximately 16%.

To determine the energy spectrum of interventional procedure by CdZnTe detector, the energy-response curve should be obtained. The ^{152}Eu and ^{133}Ba sources were usually used in the nuclear structure [20]; therefore, these sources were used to calibrate the efficiency of the CdZnTe detector. The energy spectrum of ^{152}Eu, which is shown in Fig. 1, and that of ^{133}Ba were measured by the CdZnTe detector. For each peak in Fig. 1, the peak area was obtained by the fitting. The Compton scattering and background components, which were represented by the linear function, are obvious in this measurement and contribute to the area of full-energy peak. The full-energy peaks were represented by a Gaussian function. Therefore, the fitting function contains a linear and Gaussian functions. The same fitting was performed to ^{133}Ba source. Thus, the area of each full-energy peak can be obtained. Because of the limitation of energy resolution, some peaks cannot be separated, and so the intensities of the corresponding peaks were summed. The linearity of CdZnTe detector was also obtained and is shown in Fig. 2. Here, the peaks contain 59.54 keV of ^{241}Am. A linear function was used for fitting. It is obvious that the linearity of this detection system is good. The maximum deviation is approximately 2.9% for 39.4 keV of ^{152}Eu. The deviations of other peaks were less than 1.0%.

According to the references, intensity of each peak of ^{152}Eu [21] and ^{133}Ba [22] can be obtained. I_{p1}, I_{p2}, and I_{p3} represent the intensities for peak1, peak2, and peak3, respectively. The relative efficiencies ϵ_1, ϵ_2, and ϵ_3 for peak1, peak2, and peak3, respectively, can be obtained by

Table 1 Measured energy resolution for ^{137}Cs, ^{22}Na, and ^{60}Co γ sources by CdZnTe detector

Sources	Peaks (keV)	Resolution (FWHM) (%)
^{152}Eu	39.4	16.97
	121.8	5.09
	244.7	3.05
	344.3	2.77
	443.97	2.45
	778.9	1.97
	964.1	1.98
	1085.9	2.14
	1112.0	1.34
	1408.0	1.67
^{241}Am	59.5	15.39
^{22}Na	511	2.80
	1275	1.43
^{137}Cs	662	2.35
^{60}Co	1173	2.00
	1332	1.91

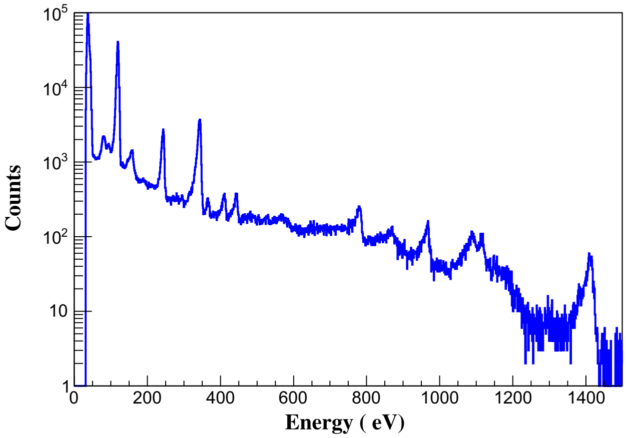

Fig. 1 The obtained energy spectrum of ^{152}Eu by CdZnTe detector

$$I_{p1} : I_{p2} : I_{p3} : \cdots = \epsilon_1 A_{p1} : \epsilon_1 A_{p1} : \epsilon_1 A_{p1} : \cdots, \qquad (1)$$

here, A_{p1}, A_{p2}, and A_{p3} denote for the peak area for peak1, peak2, and peak3, respectively. Thus, the ratio of the fitting area to intensity of ^{152}Eu and ^{133}Ba was obtained and is shown in Fig. 3. Here, the obtained ratio was normalized by the maximum value.

It is shown that the efficiency decreases sharply around 200 keV. The slope of the decrease was consistent with the simulation. The relative efficiencies at low energy were affected strongly by the thickness of entrance window of the detector. Here, the cut value for the simulation was set to 10 μm in the Geant4 toolkit. This cut value does not affect the relative efficiencies. The photoelectric effect cross section was much higher for CdZnTe at low energies. The simulated results were consistent with the measured data throughout the whole energy range. The measured data of ^{133}Ba and ^{152}Eu show a similar trend to each other. In the simulation, only the events that interacted with the detector by the photoelectric effect were recorded. In the data analysis, only the area of full-energy peak was considered for the experimental data. The experimental data agree well with the simulated results except at some points. Owing to the lack of γ sources below 30 keV, it is difficult to verify the agreement between the simulation and measurement. The present comparison indicates that the energy-response curve can be obtained by simulation for a given geometry size and energy.

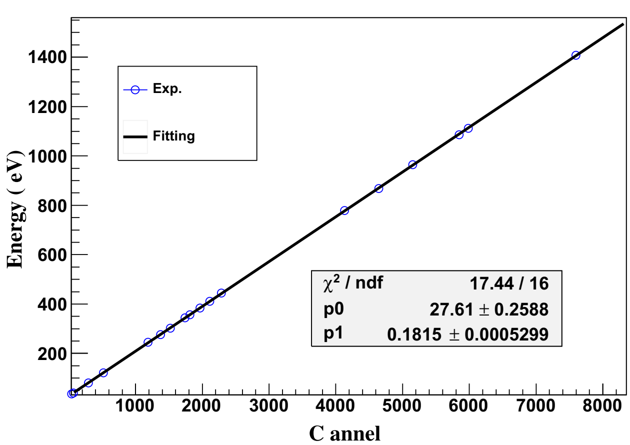

Fig. 2 The linearity of CdZnTe detector with ^{152}Eu and ^{133}Ba sources. The error bars are small compared to the symbol size and not visible

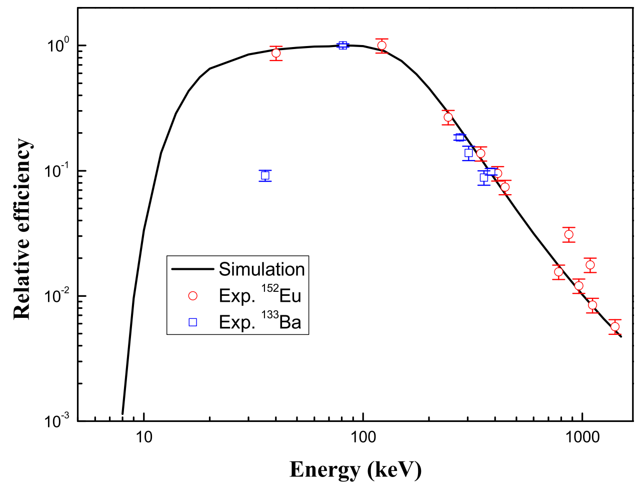

Fig. 3 The comparison of relative efficiency between the simulated results by Geant4 and measured data for CdZnTe detector with ^{152}Eu and ^{133}Ba sources. The solid line denotes the simulation results by Geant4, and the open circles and squares represent the experimental values of ^{152}Eu and ^{133}Ba, respectively. Here, the error bars of the experimental area were obtained by fitting. The error bars of the simulation originate from simulated event number. The statistical errors for simulation were approximately $1/\sqrt{10^6}$

Depending on the energy-response curve of the CdZnTe detector, the directly detected energy spectrum for the interventional procedure was corrected by the simulated curve discussed above. The corrected spectrum is shown in Fig. 4. The efficiencies for SDD and CdTe can be found in Refs. [15, 16]. The energy-response curves of the SDD and CdTe detectors were given by a series of points. These points were fitted by polynomial functions in several ranges to obtain good fitting results. The energy spectra were corrected according to the detection efficiency for the SDD and CdTe detectors, respectively. As the measurement time and efficiency were different, the obtained spectra for each detector were different. Here, we normalized the energy spectrum of SDD to connect the energy spectrum of CdTe detector. The energy spectrum combined with SDD and CdTe detectors is shown in Fig. 5. The distance to the radiation field was 7 cm for SDD and CdTe detectors. Figure 5 shows that the spectrum obtained by the CdZnTe detector is similar to the results by SDD and CdTe detectors. The peak around 20–30 keV agrees well with those by SDD and CdTe detectors. This indicates that the scattered

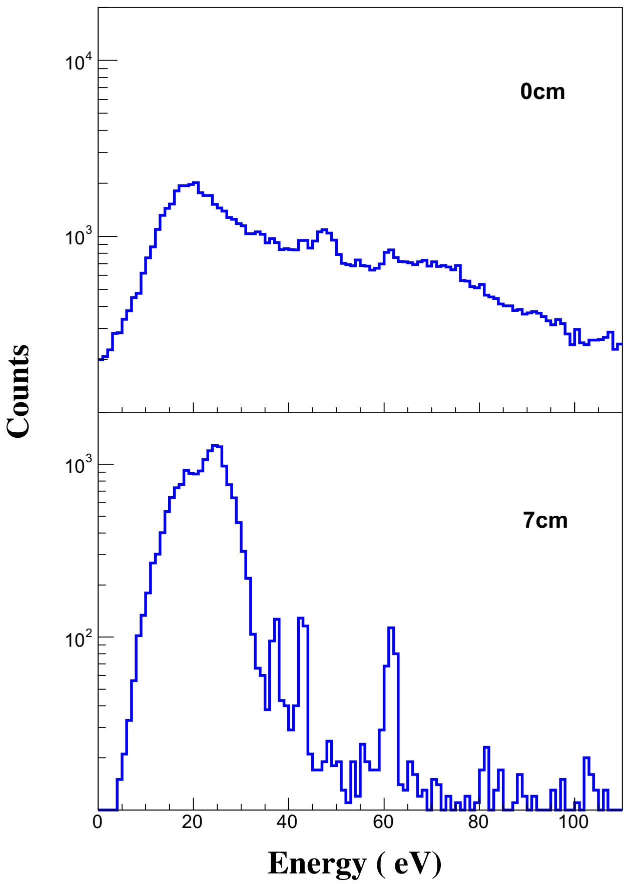

Fig. 4 Energy spectrum for interventional procedure obtained by CdZnTe. Upper one represents the measurement which is within the radiation field, and lower one represents the measurement with a distance of 7 cm to the field

X-rays contribute mostly to the energy spectrum. The energy spectra of SDD, CdTe, and CdZnTe detectors on different distances were compared. The only difference is the count rate, and the energy peak position does not change obviously; therefore, the spectra on other distances are not shown here. Compared to the CdTe detector, an obvious peak around 60 keV was observed in the measurement of CdZnTe detector. This peak originates from the Compton scattering of 73-keV X-rays, which was confirmed by the simulation. Because the efficiency of CdTe detector decreases sharply around 60 keV, this peak cannot be detected. This indicates that the CdZnTe detector is more suitable during interventional radiology procedures. The measured spectra will be meaningful to the radiation protection for occupational interventional staff.

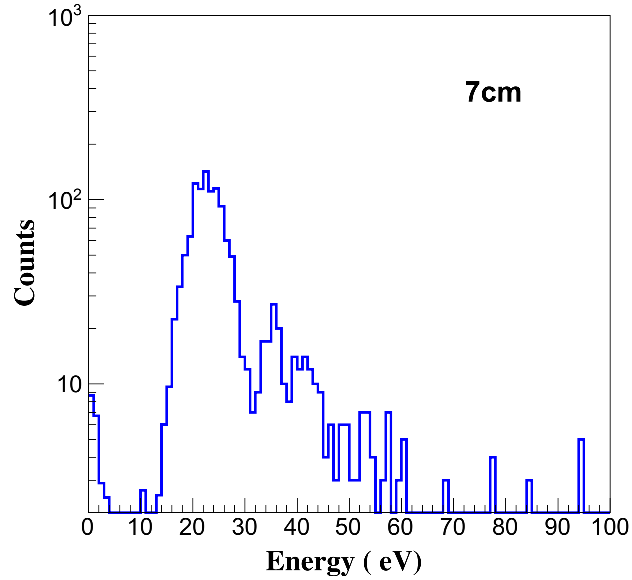

Fig. 5 Energy spectrum obtained by the SDD and CdTe detectors near the edge of the radiation field

4 Summary

The scattered X-rays contribute mostly to the occupational radiation in interventional procedures. To evaluate to doses of staff in these procedures, the measurements of energy spectra are necessary. However, the low-energy X-rays around 10–30 keV can only be detected by some semiconductor detectors. A suitable detector which can be used in interventional procedures is studied in the present paper. The energy spectra of the interventional procedures were measured by using the silicon-drift, CdTe, and CdZnTe detectors and compared. The relative efficiencies of the CdZnTe detector were simulated by the Geant4 toolkit and compared with the measurement results in this study. The measurement shows that the linearity and covered energy range of the CdZnTe detector is suitable for this application. The trend of the simulated energy-response curve of the CdZnTe detector agrees well with that of experimental results throughout the measured range. These corrected energy spectra show the true radiation environment in the interventional procedure. These measurements are meaningful for radiation protection for the staff. The relative efficiency curve plays an important role in the energy- or dose-response correction of the personal dosimeters by the CdZnTe detector.

References

1. P.O. Lopez, L.T. Dauer, R. Loose et al., ICRP publication 139: occupational radiological protection in interventional procedures. Ann. ICRP **47**, 2 (2018). https://doi.org/10.1177/0146645317750356
2. N.G.V. Pinto, D. Braz, M.A. Vallim et al., Radiation exposure in interventional radiology. Nucl. Instrum. Methods A **580**, 586–590 (2007). https://doi.org/10.1016/j.nima.2007.05.240
3. M. Barrera-Rico, X. López-Rendón, S. Vega-Montesino, I. Gamboa-deBuen, Entrance surface dose in cerebral interventional radiology procedures. Radiat. Meas. **71**, 342–348 (2014). https://doi.org/10.1016/j.radmeas.2014.04.019
4. F. O'Foghludha, G.A. Johnson, Voltage waveform effects on output and penetration of W- and Mo-anode mammographic tubes. Phys. Med. Biol. **26**, 291–303 (1981). https://doi.org/10.1088/0031-9155/26/2/008/
5. M. Matsumoto, A. Yamamoto, I. Honda et al., Direct measurement of mammographic X-ray spectra using a CdZnTe detector. Med. Phys. **27**, 1490–1502 (2000). https://doi.org/10.1118/1.599015
6. S. Miyajima, Thin CdTe detector in diagnostic X-ray spectroscopy. Med. Phys. **30**, 771–777 (2003). https://doi.org/10.1118/1.1566388
7. S. Miyajima, K. Imagawa, CdZnTe detector in mammographic X-ray spectroscopy. Phys. Med. Biol. **47**, 3959–3972 (2002). https://doi.org/10.1088/0031-9155/47/22/304
8. P. Lechner, S. Eckbauer, R. Hartmann et al., Silicon drift detectors for high resolution room temperature X-ray spectroscopy. Nucl. Instrum. Methods A **377**, 346–351 (1996). https://doi.org/10.1016/0168-9002(96)00210-0
9. P. Lechner, C. Fiorinic, R. Hartmann et al., Silicon drift detectors for high count rate X-ray spectroscopy at room temperature. Nucl. Instrum. Methods A **458**, 281–287 (2001). https://doi.org/10.1016/S0168-9002(00)00872-X
10. L. Servoli, F. Baldaccini, M. Biasini et al., Active pixel as dosimetric device for interventional radiology. Nucl. Instrum. Methods A **720**, 26–30 (2013). https://doi.org/10.1016/j.nima.2012.12.043
11. L. Servolia, L.A. Solestizia, M. Biasini et al. Real-time wireless personal dosimeter for interventional radiology procedures. Nucl. Instrum. Methods A (2018). https://doi.org/10.1016/j.nima.2018.10.184
12. S.D. Sordo, L. Abbene, E. Caroli et al., Progress in the development of CdTe and CdZnTe semiconductor radiation detectors for astrophysical and medical applications. Sensors **9**(5), 3491–3526 (2009). https://doi.org/10.3390/s90503491
13. A. Tomal, D.M. Cunha, M. Antoniassi, M.E. Poletti, Response functions of Si(Li), SDD and CdTe detectors for mammographic X-ray spectroscopy. Appl. Radiat. Isot. **70**, 1355–1359 (2012). https://doi.org/10.1016/j.apradiso.2011.11.044
14. X. Chen, H. Han, G. Li, Experimental study on high dose rate response of cadmium zinc telluride detectors to pulsed X-ray. Radiat. Meas. **97**, 42–46 (2017). https://doi.org/10.1016/j.radmeas.2016.12.015
15. Website of X-123SDD Complete X-Ray Spectrometer with Silicon Drift Detector (SDD)
16. Website of X-123CdTe Complete X-Ray & Gamma Ray Spectrometer
17. Website of Imdetec Co., LTD
18. S. Agostinelli, J. Allison, K. Amako et al., Geant4: simulation toolkit. Nucl. Instrum. Methods A **506**, 250–303 (2003). https://doi.org/10.1016/S0168-9002(03)01368-8
19. R. Brun, F. Rademakers, ROOT: an object oriented data analysis framework. Nucl. Instrum. Methods A **389**, 81–86 (1997). https://doi.org/10.1016/S0168-9002(97)00048-X
20. G.L. Zhang, G.X. Zhang, S.P. Hu et al., One-neutron stripping processes to excited states of ^{90}Y in the ^{89}Y(^{6}Li, ^{5}Li)^{90}Y* reaction. Phys. Rev. C **97**, 014611 (2018). https://doi.org/10.1103/PhysRevC.97.014611
21. M.J. Martin, Nuclear Data Sheets **114**, 1497–1847 (2013). https://doi.org/10.1016/j.nds.2013.11.001
22. Yu. Khazov, A. Rodionov, F.G. Kondev, Nuclear Data Sheets **112**, 855–1113 (2011). https://doi.org/10.1016/j.nds.2011.03.001